The HKU Scholars Hub   The University of Hong Kong   香港大學學術庫

Title	**Solution-based growth of ZnO nanorods for light-emitting devices: Hydrothermal vs. electrodeposition**
Author(s)	**Ng, AMC; Chen, XY; Fang, F; Hsu, YF; Djuriši, AB; Ling, CC; Tam, HL; Cheah, KW; Fong, PWK; Lui, HF; Surya, C; Chan, WK**
Citation	**Applied Physics B: Lasers And Optics, 2010, v. 100 n. 4, p. 851-858**
Issued Date	**2010**
URL	**http://hdl.handle.net/10722/124037**
Rights	**Creative Commons: Attribution 3.0 Hong Kong License**

Solution-based growth of ZnO nanorods for light-emitting devices: hydrothermal vs. electrodeposition

**A.M.C. Ng · X.Y. Chen · F. Fang · Y.F. Hsu ·
A.B. Djurišić · C.C. Ling · H.L. Tam · K.W. Cheah ·
P.W.K. Fong · H.F. Lui · C. Surya · W.K. Chan**

Abstract ZnO nanorods have been grown by two inexpensive, solution-based, low-temperature methods: hydrothermal growth and electrodeposition. Heterojunction n-ZnO nanorods/p-GaN light-emitting diodes have been studied for different nanorod growth methods and different preparation of the seed layer. We demonstrate that both the nanorod properties and the device performance are strongly dependent on the growth method and seed layer. All the devices exhibit light emission under both forward and reverse bias, and the emission spectra can be tuned by ZnO nanorod deposition conditions. Electrodeposition of rods or a seed layer results in yellow emission, while conventional hydrothermal growth results in violet emission.

A.M.C. Ng · X.Y. Chen · F. Fang · Y.F. Hsu · A.B. Djurišić (✉) ·
C.C. Ling
Department of Physics, The University of Hong Kong, Pokfulam
Road, Hong Kong, P.R. China
e-mail: dalek@hku.hk
Fax: +852-2559-9152

H.L. Tam · K.W. Cheah
Department of Physics, Hong Kong Baptist University, Waterloo
Road, Kowloon Tong, Hong Kong, P.R. China

P.W.K. Fong · H.F. Lui · C. Surya
Department of Electronic and Information Engineering, Hong
Kong Polytechnic University, Hung Hom, Kowloon, Hong Kong,
P.R. China

W.K. Chan
Department of Chemistry, The University of Hong Kong,
Pokfulam Road, Hong Kong, P.R. China

1 Introduction

Among various candidates for the development of short-wavelength light-emitting diodes (LEDs), ZnO and GaN are among the most promising ones due to their wide direct band gaps and relatively small lattice mismatch. In addition, ZnO nanomaterials have the important advantage that they can be fabricated using a variety of methods, and their morphology and optical properties can be varied over a wide range [1]. Consequently, various LEDs based on p-GaN/n-ZnO heterojunctions have been reported recently [2–24]. These include devices based on different ZnO morphologies, such as films [4, 5, 7–10, 12, 16–19] and nanowires [2, 3, 6, 11, 13–15, 20, 21]. While p-GaN/n-ZnO heterojunctions can be fabricated both with thin films and nanowires, nanorods/nanowires are expected to have higher efficiency [3, 11].

Devices based on ZnO nanorods/nanowires included both ZnO grown by vapor deposition [2, 6, 11, 13–15] and solution-based techniques [3, 20, 21]. Vapor-deposited ZnO nanostructures are expected to have better crystal quality compared to those prepared by solution-based techniques [1]. However, solution-based growth has important advantages of being a low-cost, low-temperature, simple process [3]. Both devices based on vapor-deposited [2] and hydrothermally grown [3] ZnO nanowires exhibited light-emission visible to the naked eye at ∼10 V, but the emission colors (blue [2] and violet and green [3]) were quite different. In general, a variety of emission colors (different combinations of UV, violet, blue, green, and yellow emission peaks) have been reported in the literature for ZnO-based LEDs [2–24]. Furthermore, in addition to devices lighting up under forward bias [2, 3], emission under reverse bias only [13], and both forward and reverse bias [18–20] have been reported. Thus, due to large differences in the reported performances for p-GaN/n-ZnO-based devices, there is considerable interest in studying their performance, in particular

in the case of ZnO fabricated by low-cost, low-temperature methods.

We have recently found that the performance of p-GaN/n-ZnO nanorod devices with hydrothermally grown nanorods is strongly dependent on the nanorod properties, as well as the properties of p-GaN substrate [20]. The properties of the nanorods have been varied by annealing [20], and it was established that different emission colors likely originate from differences in energy band alignment across GaN/ZnO interface. Since the solution-based growth methods for nanorods typically include seed layer for nanorod nucleation which is located at the interface [20], the properties of seed layer could have significant effect on the device performance. Furthermore, since nanorods could also be grown without a seed layer on a substrate with relatively small lattice mismatch such as GaN, it is also necessary to consider the growth without a seed layer.

It has been previously shown that the type of seed layer affects the morphology and alignment, as well as optical and electronic properties of the ZnO nanorods [25–27]. For vapor-deposited ZnO nanorods, the seed layer affected the I–V curves and turn-on voltages, but not the emission spectra [23]. However, the effect of the seed layer on the performance of LEDs with solution-based growth of nanorods has not been investigated.

The defects and interface states could also be affected by the presence of a seed layer and/or its method of preparation. The seed layer is expected to have a significant effect, not only due to the change of the nanorod properties, but also due to differences in GaN/ZnO interface quality. The interface quality significantly affects GaN/ZnO heterojunctions [6], therefore defects and interface states are expected to have a significant effect on the energy level alignment, carrier injection and recombination at the interface, and consequently the device performance. It has been proposed that energy band alignment in GaN film/ZnO film and GaN film/ZnO nanowire structures is different and that in case of nanowires there is a lower interfacial defect density [6].

Thus, we have investigated the performance of ZnO-GaN LED for different fabrication methods. We studied devices with ZnO nanorods grown directly by electrodeposition without a seed layer (ED sample), ZnO rods grown by a hydrothermal method on an electrodeposited seed layer (ED-HT sample) and ZnO rods grown by a hydrothermal method on a seed layer deposited from zinc acetate solution (AD-HT sample). Light emission was observed under both forward and reverse bias in all devices, but the emission spectra, I–V and C–V curves exhibited significant differences. Under reverse bias, light emission was visible by a naked eye at bias voltages as low as 4–6 V.

2 Experimental

2.1 Nanorod fabrication

In all cases, ZnO nanorods were grown on p-GaN layer deposited on sapphire substrates using metal organic chemical vapor deposition (MOCVD). 680 nm of Mg:GaN p-type layer was deposited on top of structure consisting of 500 nm highly resistive Mg:GaN/2.2 μm undoped GaN layer/30 nm GaN nucleation layer/sapphire substrate. The samples were activated by annealing in nitrogen at 825°C. After activation, hole concentration determined by Hall measurement was ∼2×10^{17} cm^{-3}. For electrodeposited rods, the synthesis solution was composed of 3.8 mM (0.034 g) zinc nitrate hydrate (Zn(NO$_3$)$_2$·xH$_2$O, 99.999%, Aldrich) and 6 mM (0.025 g) hexamethylenetetramine (HMT, C$_6$H$_{12}$N$_4$, 99%, Aldrich) in deionized water (30 ml), and the two electrode deposition setup was employed. A platinum foil was used as the anode, while the p-GaN was used as the cathode. The solution was heated up to 80°C, and then voltage of 10 V was applied, and both temperature and voltage were maintained constant for 30 min. deposition time.

For hydrothermally grown rods [25–30], two types of seed layer, one electrodeposited and one derived from zinc acetate solution, were used. For ED seed, 40 mM (0.24 g) Zn(NO$_3$)$_2$·xH$_2$O and 16 mM (0.045 g) HMT solution in ethanol:deionized water (1:1, 10 ml each) was heated up to 85°C . Zinc foil was the anode, p-GaN was the cathode, and the deposition was performed for 1 min at a voltage of 1 V. Acetate-derived seed was prepared using ethanol solution of zinc acetate [25, 26] (6 cycles of placing solution droplets, rinsing and drying, followed by annealing at 350°C for 20 min, and then entire procedure was repeated to ensure complete coverage of the substrate). After the seed layer preparation, in both cases the substrate was transferred to the solution for hydrothermal growth, which was 25 mM solution of zinc nitrate hydrate (0.56 g) and HMT (0.26 g) in deionized water (75 ml) with the addition of 0.1 g polyethylenimine (PEI, 50 wt.%). The temperature was set to 90°C and the reaction time was 2.5 hours.

2.2 Nanorod characterization

The morphology of the nanorods was examined using a JEOL JSM-7001F SEM. For photoluminescence measurements, a HeCd laser (wavelength 325 nm) was used as an excitation source and the spectra were collected using a PDA-512_USB (Control Development Inc.) fiberoptic spectrometer. The PL spectra of the GaN/ZnO heterojunctions were measured from the top (ZnO side). The PL spectra of bare p-GaN substrates were measured both from the top (p-GaN) and back (sapphire) sides of the substrate. Since the PL spectra of heterojunctions are dominated by p-GaN emission, ZnO samples were also prepared on indium tin oxide/quartz substrates for PL measurements of ZnO only.

2.3 Device fabrication and characterization

The LED and C–V measurement device structure was Au (70 nm)/Ni (30 nm)/GaN/ZnO nanorods + spin-on-glass (SOG, Futurex, Inc.)/Ag (200 nm). SOG solution was spin-coated at 3000 rpm for 40 s, followed by annealing at 200°C for 1 min. The spinning conditions have been optimized to ensure minimum SOG coverage at the top of the nanorods, by varying the spinning conditions and observing the resulting samples by SEM and measuring their I–V curves. Furthermore, the SOG solution should be fresh since the solvent evaporates over storage time and thus concentration increases, resulting in a thick SOG layer. It should be noted that the specified spin-coating condition has been optimized for substrate size of ∼1 cm × 1.5 cm. Different substrate sizes, quantity of dispensed liquid, etc. may result in differences in SOG coverage on the nanorods, and thus spin-coating conditions should be carefully calibrated for the substrate and spin-coater used. The function of the SOG layer is to fill the space between the rods and prevent direct contact of the top electrode and p-GaN layer. Different insulating layers can be used for this purpose, such as poly(methyl methacrylate) [2, 3] and photoresist [13]. All the electrodes were evaporated in high vacuum through a shadow mask (1 mm radius) using a thermal evaporator AST PEVA 500 EL. Ni/Au contact has been used as a contact for p-GaN (and verified to form an ohmic contact with p-GaN, i.e. linear I–V curves are obtained). Ag has been used as an ohmic contact for ZnO nanorods, and linear I–V curves are also obtained for Ag/ZnO nanorods+SOG/Ag structure. EL measurements were performed using a Keithley 2400 source meter to provide fixed voltage bias, and the emission spectra were collected using a monochromator (Acton SpectraPro 500i) with Peltier-cooled photomultiplier detector (Hamamatsu R636-10). C–V measurements were performed using a HP 4275A Multi-frequency LCR meter at a frequency of 1 MHz.

3 Results and discussion

Figure 1 shows SEM images of the nanorods grown by different solution-based procedures. Both AD and ED seed layers result in very thin (<50 nm) islands on the substrate, which can then serve as nucleation centers for the nanorod growth by hydrothermal method. The seed layer had a significant effect on the density of the rods. AD seed layer results in dense coverage of nanorods across entire substrate, while for both ED and ED-HT samples, nanorods are less dense and some variations in the density from one area to another are observed. In all cases, the rods exhibit good alignment perpendicular to the substrate. It has been shown previously that the seed layer affects the alignment of the
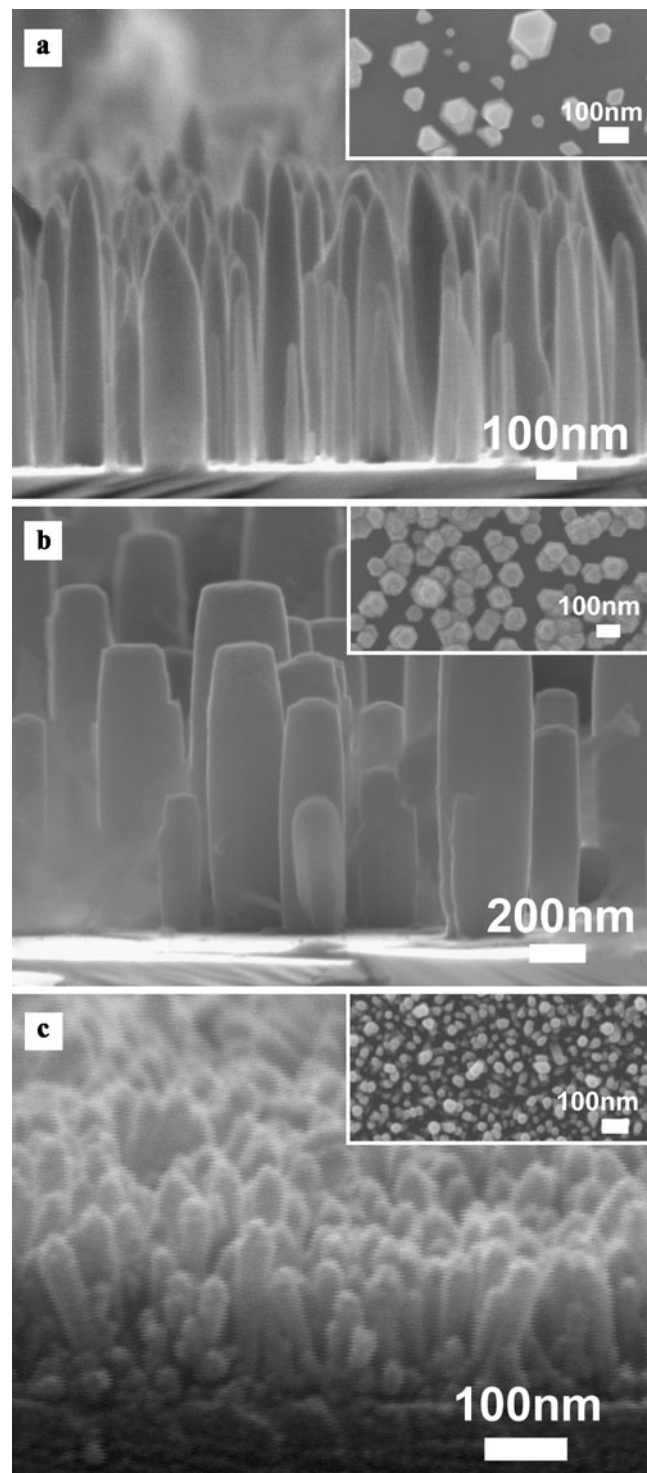

Fig. 1 SEM images of the cross-section view ZnO nanorods fabricated by different methods, with the *inset* showing the top view. (**a**) ED-HT (**b**) ED (**c**) AD-HT

nanorods [26, 27, 29, 30], and the nanorod size is affected by the grain size in the seed layer/deposition conditions for the seed layer [27, 29, 30]. However, in addition to the rod density, the seed layer and the rod growth method affect the rod
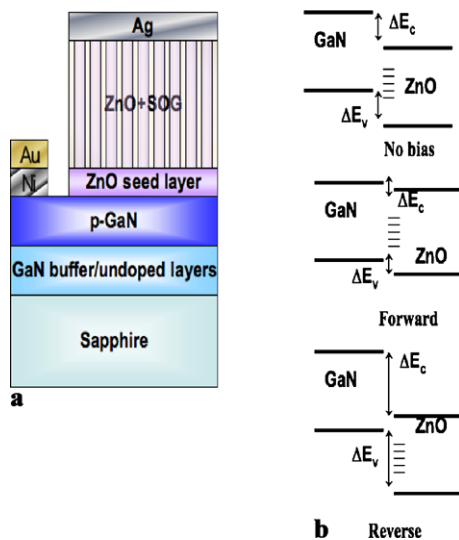
Fig. 2 (**a**) Device diagram and (**b**) schematic energy band diagram of p-GaN/n-ZnO heterojunction devices

shape. While majority of the rods exhibit hexagonal cross-section, change in the rod diameter (narrowing near the top) in ED-HT rods can be observed. The reasons for the decrease in diameter near the top are not fully clear. However, a previous report of the ZnO nanorods on GaN grown by a hydrothermal method has also shown relatively low density of the nanorods, and gradual decrease of nanorod diameter towards the tip [3].

The ZnO nanorods grown by different solution-based procedures have been used to fabricate the p-GaN/n-ZnO heterojunction LEDs. The device diagram and schematic energy band diagram are shown in Fig. 2, while the I–V and C–V curves are shown in Fig. 3. The inset of Fig. 3a shows that ohmic contacts to p-GaN have been achieved. Figure 3b shows that ohmic contacts to ZnO nanorods (with SOG) have been achieved, which indicates that the coverage of SOG on the top of the nanorod for optimal spin-coating conditions is negligible (otherwise rectifying I–V curve would be obtained). In addition, the devices are lighting up uniformly over a defined device area (under Ag contact), which confirms the quality of the devices. Poor contact quality or light emission from direct injection of carriers into the GaN layer results in devices lighting up at the contact edge, rather than uniformly under the Ag contact to ZnO. Contact problems can also result in a spotty instead of uniform emission.

The PL and EL spectra of the devices under forward and reverse bias, as well as representative device photos, are shown in Fig. 4. PL spectra of all devices are similar, with the emission spectrum dominated by a blue emission peak from p-GaN layer centered at ∼440 nm. There is a weak orange emission (stronger for AD-HT sample, compared to ED-HT and ED samples), which originates from the defects in ZnO [1, 28, 31]. To observe the emission from ZnO in more detail, ZnO nanorods on ITO/quartz have
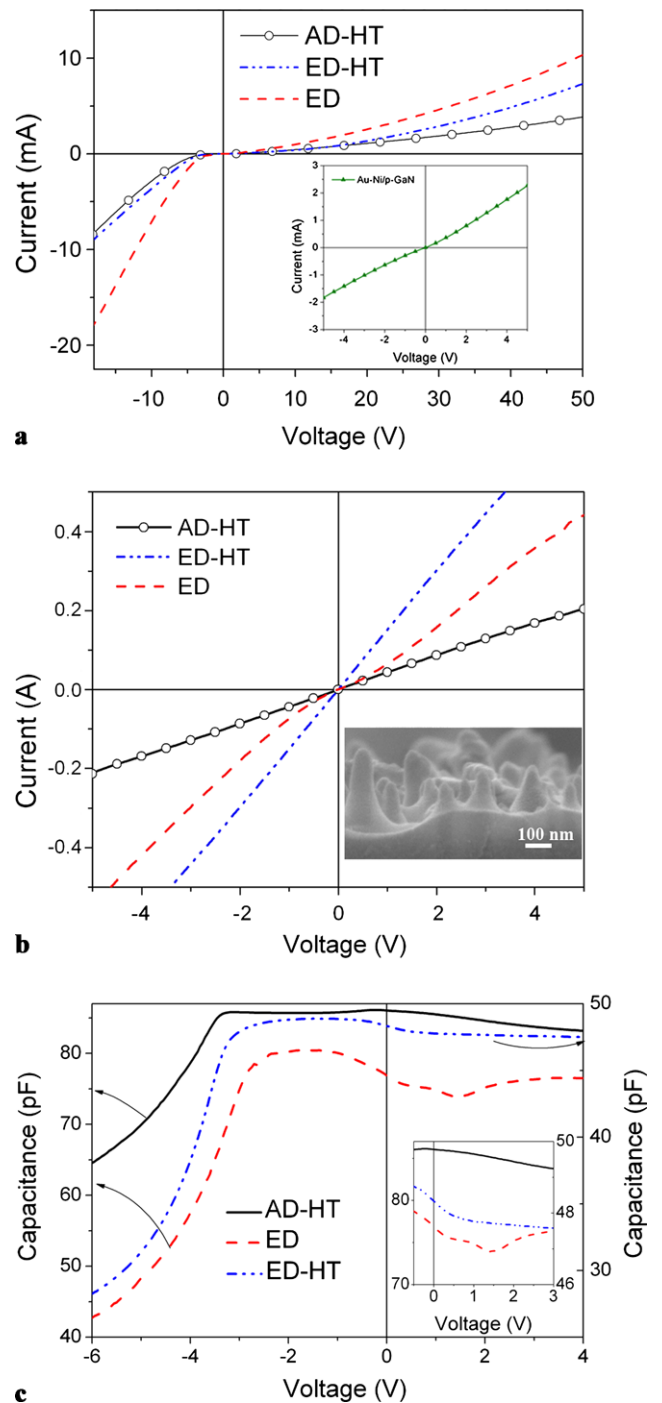

Fig. 3 (**a**) I–V curves for different devices. The *inset* shows that ohmic contacts to p-GaN have been achieved. (**b**) I–V curves for ITO/Ag/ZnO nanorod+SOG/Ag devices demonstrating that ohmic contact n-ZnO have been achieved. The *inset* shows an SEM image of ZnO nanorods+SOG (ED-HT sample). (**b**) C–V curves for different devices. C–V measurements have been done at a frequency of 1 MHz. The *inset* shows enlarged positive bias part of the graph

been prepared and their PL spectra are shown in Fig. 5. All the samples exhibit prominent orange and weak UV emission with similar ratios of UV-to-visible emission, although

Fig. 4 (**a**) PL spectra from p-GaN/n-ZnO heterojunctions. PL spectrum from p-GaN substrate, measured both from p-GaN film side (front) and sapphire substrate side (back) is shown for comparison. (**b**) EL spectra from different devices at forward bias (16 V for AD-HT, 55 V for ED and ED-HT). (**c**) EL spectra from different devices at reverse bias (−12 V for all devices). The insets show device photos. (**d**) EL spectra of AD-HT device at different reverse bias voltages. All spectra have been normalized for easier comparison of emission peak positions
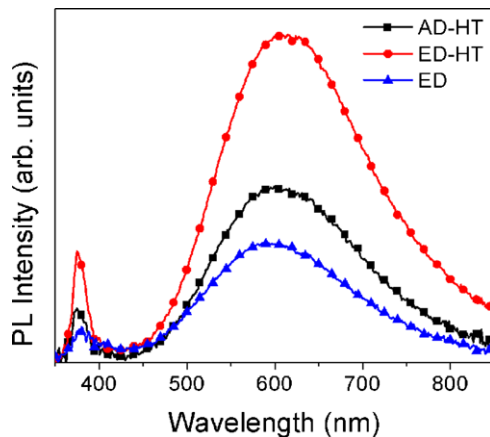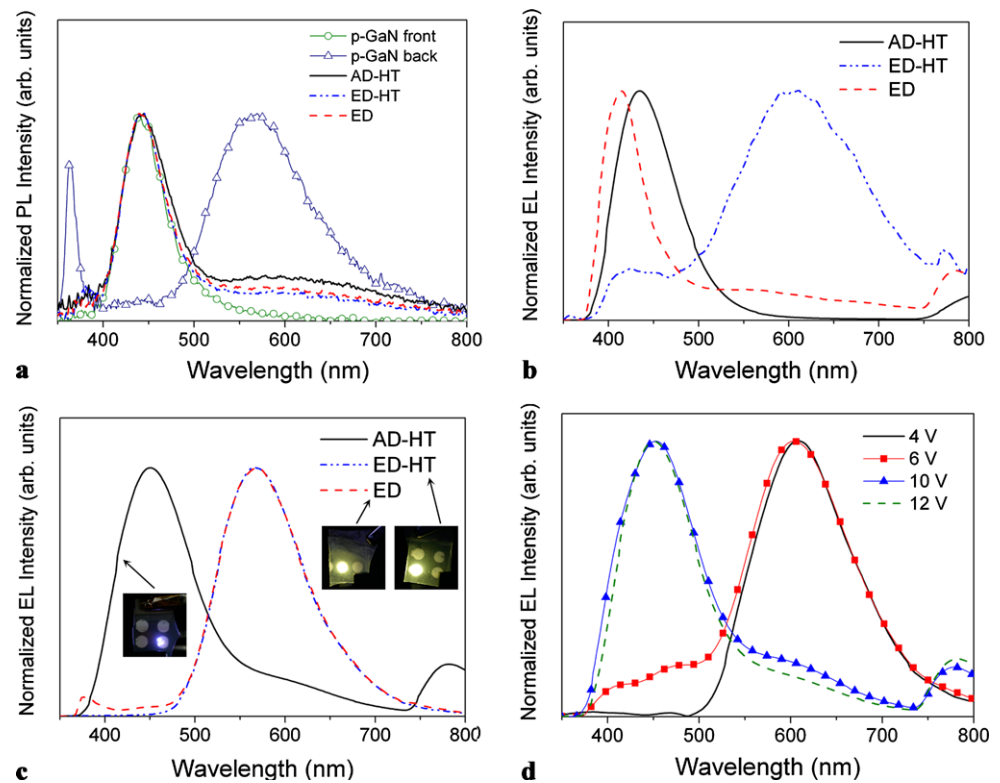

Fig. 5 PL spectra from ZnO nanorods on ITO/quartz substrates

overall emission intensities were different. The orange defect emission is commonly observed in samples grown by solution-based methods [1, 28, 31]. Although its exact origin has not been conclusively established, it was attributed to defect complexes and it was found to be related to the presence of adsorbates, such as OH groups, on the rod surface [31]. Explanations proposed to explain orange luminescence also include oxygen interstitials, since this emission is reduced by annealing in vacuum or hydrogen/argon gas mixture [28]. However, it should be noted that GaN also exhibits defect emissions (yellow and red) in a similar spectral range [32, 33]. Yellow defect emission in GaN has been attributed

to transitions from conduction band or a shallow donor to a deep acceptor [32, 33]. In this case as well the exact identity of the acceptor has not been conclusively established, but there is evidence indicating that this acceptor defect is likely a gallium vacancy [33]. This emission band is usually suppressed in p-GaN [33], and in agreement with that in Fig. 4a we can observe that yellow emission from the GaN substrate is negligible when excited from p-GaN side and prominent when excited from substrate/n-GaN side. Red luminescence band (1.5–2.0 eV) is less common than yellow emission and several different defects could possibly contribute to this emission band [33]. In heavily Mg doped p-GaN, red emission band can occur due to deep donor-deep acceptor transition [33]. It was also proposed that red emission bands originate from near-surface region, and that the yellow band is also enhanced near the surface compared to the bulk [32].

In addition to similarities in the optical properties of devices with different ZnO nanorods, there are also similarities in the shape of the I–V curves (Fig. 3a). We can observe that I–V curves are non-linear, but the shape of the curves is different from a conventional p–n junction. Previous reports of p-GaN/n-ZnO heterojunctions include good rectifying properties [3, 4, 6, 10, 11], as well as poor rectification and almost symmetric I–V curves [7–10, 12, 14, 16–19]. Inferior rectification properties have in some cases been attributed to the existence of defects [12]. In our case, the obtained I–V curves are not symmetric and resemble

backward diode I–V curves [34]. In a backward diode, tunneling component of the current is dominant in the reverse direction [34], and such behavior was reported in different heterojunctions [35, 36]. This situation can occur when one side of the junction is more heavily doped [34]. Carrier concentration in ZnO nanorods grown by solution methods is usually rather high, of the order $\sim 10^{19}$ cm^{-3} for electrodeposited nanorods [37] and $\sim 10^{18}$ cm^{-3} for hydrothermally grown nanorods [38]. In agreement with that, both HT samples exhibit smaller current for the same bias voltage compared to ED sample. However, for both growth methods the electron concentration in undoped ZnO could be higher than the hole concentration in p-GaN layer, which is typically of the order 10^{17} cm^{-3}. Therefore, such situation could occur in GaN/ZnO heterojunctions and account for behavior observed in our work, as well as previous reports [13, 18, 20, 23]. Also, backward diode characteristics occurs when energy band alignment across the interface favors tunneling, and this is consistent with expected energy level alignment at GaN/ZnO interface and observed EL behavior [13, 18, 20].

C–V curves of the devices (Fig. 3c) exhibit fewer similarities among each other compared to the I–V curves. The differences in the obtained capacitance values are likely due to differences in rod density and rod length for different methods in addition to differences in their charge transport properties. However, we can also observe differences in the shape of the C–V curves, and the shape of the curves is dependent on the distribution of the interface states [39]. Changes in the slope of C–V curves observed in some of the devices (ED) could occur both from carrier concentration changes as well as abrupt changes in the rod diameter. From the C–V curves shown in Fig. 3c, we can conclude that in all devices there are likely significant trapped charges at the interface. Large charge density at a GaN/ZnO interface is expected to result in a large band offset [40]. While small offsets of $\Delta E_c = 0.12$ eV and $\Delta E_v = 0.15$ eV based on Anderson model has been proposed [5, 7, 15], more comprehensive calculations predict significant band offsets, from 1.0 to 2.2 eV, with larger offsets in presence of interface charges [41]. Experimental findings also confirm relatively large band offsets, $\Delta E_v = 0.4$–0.5 [42], and $\Delta E_v = 0.8$ [43], and $\Delta E_c = 0.5$–0.6 eV [42]. The offsets were found to be dependent on the growth conditions [42], as well as the polarity of ZnO [43]. In all cases, type II energy band alignment is obtained, as illustrated in Fig. 2b. It should also be noted that large energy band offset would favor tunneling, which is consistent with observed backward diode behavior.

Due to variations in native defects and trapped charges for different seed layers/fabrication conditions, the differences in GaN/ZnO interface energy band alignments are expected to occur. This is expected to result in differences in

carrier recombination and consequently different emission spectra. It should also be noted that while the lattice mismatch ($\sim 1.8\%$) [5] between GaN and ZnO is considered relatively low, in heterojunctions with lattice mismatch $>1\%$ interface states dominate the current flow mechanisms [44]. We have indeed observed considerable differences in the emission spectra of the devices. All the devices light up under both forward and reverse bias, but at different bias voltages. Obtained turn-on voltages, defined as observation of light emission by naked eye, are comparable [13, 15] or lower [2, 3] than previously reported values. The turn-on voltage for AD-HT device was 4 V in reverse bias, 10 V in forward bias (forward bias turn-on voltage and dominant violet-blue emission were similar to that previously reported for hydrothermally grown ZnO nanorods [3]). For ED and ED-HT devices, turn-on voltages were 5.5–6 V under reverse bias, and ~ 30 V under forward bias. Lighting up under both forward and reverse bias has been previously observed in other heterojunctions, such as ZnO/p-Si [45] and p-Si/AlN [46] in addition to ZnO/GaN based heterojunctions [18–20, 23]. While in ZnO/ZnO:SiO$_2$/GaN devices UV emission (373 nm) under reverse bias appeared due to impact ionization at reverse breakdown bias [19], and blue emission in p-Si/AlN junctions was attributed to carrier injection from metal contact into deep levels in AlN [46], in other cases light emission under reverse bias was attributed to tunneling [13, 18, 20, 45]. Thus, the emission under reverse bias is likely due to tunneling across the heterojunction which occurs in the case of large band offsets [13, 18, 20], and which is consistent with the observed backward diode behavior [34] and the indications of significant trapped charges in C–V curves.

The emission spectra from the devices were different under forward and reverse bias, in agreement with previous reports [18, 20]. We have obtained violet (ED), blue-violet (AD-HT) and yellow (with small violet contribution, ED-HT) emission under forward bias, and yellow (ED, ED-HT) and violet (AD-HT) emissions under reverse bias. Blue-violet emission, believed to predominantly originate from recombination in p-GaN layer, with a weak contribution from ZnO defect emission under forward bias was previously reported for hydrothermally grown ZnO nanowires [3]. Yellow emission peak was previously attributed to defects in ZnO [13] and lattice defects in GaN [21, 22, 24]. Considering the fact that yellow emission under reverse bias was also observed in devices which exhibited green defect emission PL from ZnO [23], it is possible that yellow emission indeed originates either from GaN or the interface between GaN and ZnO. Since the yellow emission in GaN exhibits higher intensity in near-surface region [32], the interface between the two materials is expected to have higher defect concentration. The origin of the violet emission centered around 400 nm is less clear since there are no

corresponding peaks in the PL spectra of both p-GaN and ZnO. Therefore, this emission could originate from interface recombination, since EL occurs in the region near the interface while PL is probing the region within optical penetration depth from the surface.

In addition to differences in the emission spectra of different devices, they also exhibit different behavior with increasing bias voltage. While there is no change in peak positions in ED and ED-HT devices, for AD-HT devices we observed small blue shift with increasing forward bias voltage, while for reverse bias the emission spectra change from dominant yellow emission (4 V), over spectra with increasing violet-blue component (6 V) to spectra with dominant violet-blue component (10 V, 12 V), as shown in Fig. 4d and similar to previously reported results [13]. Differences in the dependence of the emission spectra on bias voltage compared to previous work [20] are likely due to different p-GaN substrate used.

Thus, the seed layer and growth method mainly affect the nanorod morphology and density and ZnO/GaN interface properties. PL spectra of all the nanorods exhibited orange and UV emissions, with similar UV-to-visible emission ratios. Ratio of UV-to-visible emission is frequently used as an indicator of sample quality and defect concentrations [1]. While this ratio is dependent on the measurement parameters, such as excitation density and area, for measurements performed under identical conditions it can be used for comparison of the quality of different samples [1]. Therefore, since all the nanorods exhibit similar UV-to-visible emission ratios, they likely have similar crystal quality.

However, the emission spectra of the devices exhibited significant differences. Since the recombination processes in GaN/ZnO heterojunctions are expected to be significantly affected by the interface [44], differences in the EL spectra indicate differences in the interface states for ZnO preparation methods used. The fact that ED and ED-HT samples exhibit similar I–V curves and electroluminescence further indicates that the fabrication method has significant influence on the interface quality and existence of interface states (since in both samples electrodeposition was used). Thus, the emission spectrum of GaN/ZnO heterojunctions can be controlled by changing the seed layer for nanorod growth and thus affecting energy band alignment across the interface. Since large band offsets are expected for this materials system and both materials can exhibit a variety of defect states, a wide range of observed device behaviors is possible, which can account for a large variety of device performance reports for GaN/ZnO LEDs.

4 Conclusions

In summary, we fabricated p-GaN/n-ZnO nanorod LEDs which exhibited low turn-on voltages under reverse bias. The light emission was observed under both forward and reverse biases. The emission color (violet, blue, yellow) could be changed by changing the seed layer and/or growth method for the ZnO nanorods. Observed variations for devices with different nanorods were attributed to the differences in interface states and the energy band alignment across GaN/ZnO interface.

References

1. A.B. Djurišić, Y.H. Leung, Small **2**, 944 (2006)
2. X.-M. Zhang, M.-Y. Lu, Y. Zhang, L.-J. Chen, Z.L. Wang, Adv. Mater. **21**, 2767 (2009)
3. E. Lai, W. Kim, P.D. Yang, Nano Res. **1**, 123 (2008)
4. S.-H. Hwang, T.-H. Chung, B.-T. Lee, Mat. Sci. Eng. B **157**, 32 (2009)
5. T.P. Yang, H.C. Zhu, J.M. Bian, J.C. Sun, X. Dong, B.L. Zhang, H.W. Liang, X.P. Li, Y.G. Cui, G.T. Du, Mater. Res. Bull. **43**, 3614 (2008)
6. R. Guo, J. Nishimura, M. Matsumoto, M. Higashihata, D. Nakamura, T. Okada, Appl. Phys. B **94**, 33 (2009)
7. J.W. Sun, Y.M. Lu, Y.C. Liu, D.Z. Shen, Z.Z. Zhang, B.H. Li, J.Y. Zhang, B. Yao, D.X. Zhao, X.W. Fan, J. Phys. D, Appl. Phys. **41**, 155103 (2008)
8. L. Zhao, C.S. Xu, Y.X. Liu, C.L. Shao, X.H. Li, Y.C. Liu, Appl. Phys. B **92**, 185 (2008)
9. R.W. Chuang, R.-X. Wu, L.-W. Lai, C.-T. Lee, Appl. Phys. Lett. **91**, 231113 (2007)
10. C.P. Chen, M.Y. Ke, C.C. Liu, Y.J. Chang, F.H. Yang, J.J. Huang, Appl. Phys. Lett. **91**, 091107 (2007)
11. M.-C. Jeong, B.-Y. Oh, M.-H. Ham, S.W. Lee, J.M. Myong, Small **3**, 568 (2007)
12. Ya.I. Alivov, J.E. Van Nostrand, D.C. Look, M.V. Chukichev, B.M. Ataev, Appl. Phys. Lett. **83**, 2943 (2003)
13. W.I. Park, G.-C. Yi, Adv. Mater. **16**, 87 (2004)
14. S.-H. Park, S.-H. Kim, S.-W. Han, Nanotechnology **18**, 055608 (2007)
15. M.-C. Jeong, B.-Y. Oh, M.-H. Ham, J.M. Myong, Appl. Phys. Lett. **88**, 202105 (2006)
16. D.J. Rogers, F. Hosseini Teherani, A. Yasan, K. Minder, P. Kung, M. Razeghi, Appl. Phys. Lett. **88**, 141918 (2006)
17. H.Y. Xu, Y.C. Liu, Y.X. Liu, C.S. Xu, C.L. Shao, R. Mu, Appl. Phys. B **80**, 871 (2005)
18. Q. Qin, L.-W. Guo, Z.-T. Zhou, H. Chen, X.-L. Du, Z.-X. Mei, J.-F. Jia, Q.-K. Xue, J.-M. Zhou, Chin. Phys. Lett. **22**, 2298 (2005)
19. M.K. Wu, Y.T. Shih, W.C. Li, H.C. Chen, M.J. Chen, H. Kuan, J.R. Yang, M. Shiojiri, IEEE Photon. Technol. Lett. **20**, 1772 (2008)
20. A.M.C. Ng, Y.Y. Xi, Y.F. Hsu, A.B. Djurišić, W.K. Chan, S. Gwo, H.L. Tam, K.W. Cheah, P.W.K. Fong, H.F. Lui, C. Surya, Nanotechnology **20**, 445201 (2009)

21. I.E. Titkov, A.S. Zubrilov, L.A. Delimova, D.V. Mashovets, I.A. Liniicuk, I.V. Grekhov, Semiconductors **41**, 564 (2007)
22. I.E. Titkov, L.A. Delimova, A.S. Zubrilov, N.V. Seredova, I.A. Liniicuk, I.V. Grekhov, J. Mod. Opt. **56**, 653 (2009)
23. X.Y. Chen, A.M.C. Ng, F. Fang, A.B. Djurišić, W.K. Chan, H.L. Tam, K.W. Cheah, P.W.K. Fong, H.F. Lui, C. Surya, J. Electrochem. Soc. **157**, H308 (2010)
24. S.H. Hwang, T.H. Chung, B.T. Lee, Mater. Sci. Eng. B **157**, 32 (2009)
25. Y.F. Hsu, Y.Y. Xi, K.H. Tam, A.B. Djurišić, J. Luo, C.C. Ling, C.K. Cheung, A.M.C. Ng, W.K. Chan, X. Deng, C.D. Beling, S. Fung, K.W. Cheah, P.W.K. Fong, C. Surya, Adv. Func. Mater. **18**, 1020 (2008)
26. L.E. Greene, M. Law, D.H. Tan, M. Montano, J. Goldberger, G. Somorjai, P.D. Yang, Nano Lett. **5**, 1231 (2005)
27. J.-S. Huang, C.-F. Lin, J. Appl. Phys. **103**, 014304 (2008)
28. L.E. Greene, M. Law, J. Goldberger, F. Kim, J.C. Johnson, Y.F. Zhang, R.J. Saykally, P.D. Yang, Angew. Chem. Int. Ed. **42**, 3031 (2003)
29. J. Song, S. Lim, J. Phys. Chem. C **111**, 596 (2007)
30. Y.F. Tao, M. Fu, A.L. Zhao, D.W. He, Y.S. Wang, J. Alloys Compd. **489**, 99 (2010)
31. A.B. Djurišić, Y.H. Leung, K.H. Tam, Y.F. Hsu, L. Ding, W.K. Ge, Y.C. Zhong, K.S. Wong, W.K. Chan, H.L. Tam, K.W. Cheah, W.M. Kwok, D.L. Phillips, Nanotechnology **18**, 095702 (2007)
32. I.M. Huygens, W.P. Gomes, K. Strubbe, J. Electrochem. Soc. **153**, G72 (2006)
33. M.A. Reshchikov, H. Morkoç, J. Appl. Phys. **97**, 061301 (2005)
34. K.K. Ng, *Complete Guide to Semiconductor Devices* (Wiley, New York, 2002)
35. G. Li, T.F. Zhou, D.D. Hu, Y.P. Pao, Y. Hou, X.G. Li, Appl. Phys. Lett. **91**, 163114 (2007)
36. T. Phetchakul, H. Kimura, Y. Akiba, T. Kurosu, M. Iida, Jpn. J. Appl. Phys. **35**, 4247 (1996)
37. I. Mora-Seró, F. Fabregat-Santiago, B. Denier, J. Bisquert, R. Tena-Zaera, C. Lévy-Clément, Appl. Phys. Lett. **89**, 203117 (2006)
38. M. Law, L.E. Greene, J.C. Johnson, R.J. Saykally, P.D. Yang, Nat. Mater. **4**, 455 (2005)
39. N.I. Bochkareva, E.A. Zhirnov, A.A. Efremov, Yu.T. Rebane, R.I. Gorbunov, A.V. Klochkov, D.A. Lavrinovich, Yu.G. Shreter, Semiconductors **39**, 795 (2005)
40. D.C. Oh, T. Suzuki, J.J. Kim, H. Makino, T. Hanada, M.W. Cho, T. Yao, H.J. Ko, Appl. Phys. Lett. **87**, 162104 (2005)
41. T. Nakayama, M. Murayama, J. Cryst. Growth **214/215**, 299 (2000)
42. H.F. Liu, G.X. Hu, H. Gong, K.Y. Zang, H.F. Chua, J. Vac. Sci. Technol. A **26**, 1462 (2008)
43. S.-K. Hong, T. Hanada, H. Makino, H.-J. Ko, Y. Chen, T. Yao, J. Vac. Sci. Technol. B **19**, 1429 (2001)
44. A.G. Milnes, D.L. Feucht, *Heterojunctions and Metal-Semiconductor Junctions* (Academic Press, New York, 1972)
45. P.L. Chen, X.Y. Ma, D.R. Yang, J. Appl. Phys. **101**, 053103 (2007)
46. J.L. Zhao, S.T. Tan, S. Iwan, X.W. Sun, W. Liu, S.J. Chua, Appl. Phys. Lett. **94**, 093506 (2009)